



Atomic diffusion in liquid gallium and gallium-nickel alloys probed by quasielastic neutron scattering and molecular dynamic simulations

A Shahzad^{1,2,3}, F Yang⁴ , J Steffen⁵, C Neiss⁵ , A Panchenko^{1,2}, K Goetz^{1,2}, C Vogel^{1,2}, M Weisser^{1,2}, J P Embs⁶, W Petry⁷, W Lohstroh⁸, A Görling⁵, I Goychuk^{1,2,*} , and T Unruh^{1,2,*} 

¹ Institute for Crystallography and Structural Physics, Friedrich-Alexander-Universität Erlangen-Nürnberg (FAU), Staudtstraße 3, Erlangen 91058, Germany

² Interdisciplinary Center for Nanostructured Films (IZNF) and Center for Nanoanalysis and Electron Microscopy (CENEM), Cauerstraße 3, Erlangen 91058, Germany

³ Institute for Material Science, University of Stuttgart, Heisenbergstr. 3, 70569 Stuttgart, Germany

⁴ Institut für Materialphysik im Weltraum, Deutsches Zentrum für Luft- und Raumfahrt (DLR), 51170 Köln, Germany

⁵ Chair of Theoretical Chemistry, FAU, 91058 Erlangen, Germany

⁶ Laboratory for Neutron Scattering and Imaging, Paul Scherrer Institut (PSI), CH-5232 Villigen, Switzerland

⁷ Physics Department, Technical University of Munich, James-Frank-Str. 1, 85747 Garching, Germany

⁸ Research Neutron Source Heinz Maier-Leibnitz (FRM II), Technical University of Munich, Lichtenbergstr. 1, 85748 Garching, Germany

E-mail: igor.a.goychuk@fau.de and tobias.unruh@fau.de

Received 8 September 2023, revised 4 January 2024

Accepted for publication 15 January 2024

Published 1 February 2024



Abstract

The atomic mobility in liquid pure gallium and a gallium-nickel alloy with 2 at% of nickel is studied experimentally by incoherent quasielastic neutron scattering. The integral diffusion coefficients for all-atom diffusion are derived from the experimental data at different temperatures. DFT-based *ab-initio* molecular dynamics (MD) is used to find numerically the diffusion coefficient of liquid gallium at different temperatures, and numerical theory results well agree with the experimental findings at temperatures below 500 K. Machine learning force fields derived from *ab-initio* molecular dynamics (AIMD) overestimate within a small 6% error the diffusion coefficient of pure gallium within the genuine AIMD. However, they better agree with experiment for pure gallium and enable the numerical finding of the diffusion coefficient of nickel in the considered melted alloy along with the diffusion coefficient of gallium and integral diffusion coefficient, that agrees with the corresponding experimental values within the

* Authors to whom any correspondence should be addressed.



Original Content from this work may be used under the terms of the [Creative Commons Attribution 4.0 licence](https://creativecommons.org/licenses/by/4.0/). Any further distribution of this work must maintain attribution to the author(s) and the title of the work, journal citation and DOI.

error bars. The temperature dependence of the gallium diffusion coefficient $D_{\text{Ga}}(T)$ follows the Arrhenius law experimentally for all studied temperatures and below 500 K also in the numerical simulations. However, $D_{\text{Ga}}(T)$ can be well described alternatively by an Einstein–Stokes dependence with the metallic liquid viscosity following the Arrhenius law, especially for the MD simulation results at all studied temperatures. Moreover, a novel variant of the excess entropy scaling theory rationalized our findings for gallium diffusion. Obtained values of the Arrhenius activation energies are profoundly different in the competing theoretical descriptions, which is explained by different temperature-dependent prefactors in the corresponding theories. The diffusion coefficient of gallium is significantly reduced (at the same temperature) in a melted alloy with natural nickel, even at a tiny 2 at% concentration of nickel, as compared with its pure gallium value. This highly surprising behavior contradicts the existing excess entropy scaling theories and opens a venue for further research.

Supplementary material for this article is available [online](#)

Keywords: self-diffusion, liquid gallium, gallium-nickel alloy, quasielastic neutron scattering, ab-initio molecular dynamics, DFT-based machine learning force fields

1. Introduction

Supported catalytically active liquid metal solutions (SCALMS) represent a new class of catalysts that intend to combine the inherent advantages of heterogeneous catalysis linked to the separated phases of the catalyst and the reactants with the possibility to achieve and optimize high activity and selectivity of single-atom catalysis [1]. In SCALMS, it is intended to provide a huge interface of solid supported liquid metal nanodroplets with active single-atom catalysts embedded in the essentially non-active liquid metal phase (e.g. liquid gallium) [2]. In contrast to solid metal nanoparticles the single-atom active sites in liquids are highly dynamic and are assumed to diffuse into the bulk of the liquid metal support and emerge at a later time at the interface again which leads to a continuous reformation of the catalytically active sites at the interface. This mechanism is expected to enhance the long-term catalyst stability and significantly reduce deactivation effects like, e.g. coking [2]. Besides noble metal single-atom catalysts, nickel has recently been proposed in Ga–Ni SCALMS for selective ethylene oligomerization [3]. In such systems, a detailed understanding of the atomic dynamics on a picosecond time scale is very important as it determines the dynamic restructuring of the catalytically active interface. In a first step, the atomic diffusion in the bulk phase of the pure liquid metal support material (e.g. Ga) and the active alloys (e.g. $\text{Ga}_{1-x}\text{Ni}_x$) used in SCALMS should be investigated for understanding the atomic transport of the active catalytic component in the liquid catalytic systems and, perspective, their influence on the catalytic reactions [4].

Incoherent quasielastic neutron scattering (QENS) [5–7] provides a powerful experimental tool to investigate diffusion in liquids [5] including liquid metals and metallic alloys [8–14]. In this paper, the results of time-of-flight (TOF) QENS experiments and molecular dynamics (MD) simulations of the self-diffusion of atoms in pure liquid Ga and a $\text{Ga}_{1-x}\text{Ni}_x$ alloy at the small Ni concentration of $x=0.02$ are presented.

2. Theoretical background

The partial differential cross-section of neutrons scattered by a system of N atoms/nuclei in a differential solid angle $\partial\Omega$ and an infinitesimal energy interval $\partial E'$ is given by a sum [5–7, 15]

$$\frac{\partial^2 \sigma}{\partial \Omega \partial E'} = \frac{N}{4\pi} \frac{|\vec{k}'|}{|\vec{k}|} \left[\sigma_{\text{coh}} S_{\text{coh}}(\vec{Q}, \omega) + \sigma_{\text{inc}} S_{\text{inc}}(\vec{Q}, \omega) \right] \quad (1)$$

of two terms. They involve the coherent, $S_{\text{coh}}(\vec{Q}, \omega)$, and incoherent, $S_{\text{inc}}(\vec{Q}, \omega)$, scattering functions, correspondingly. Here, $\vec{Q} = \vec{k} - \vec{k}'$ denotes the scattering vector which equals the difference of the wave vectors of the incident (\vec{k}) and scattered (\vec{k}') neutrons; $\hbar\omega = E - E'$ is the difference of their energies before and after the scattering event, and σ_{coh} and σ_{inc} are the coherent and incoherent averaged neutron scattering cross-sections per nucleus, correspondingly. Equation (1) is based on the assumption that no correlation of the position of a nucleus with its scattering length exists, which is assumed to hold for all systems discussed in this contribution.

Fundamentally, the coherent cross-section is related to the average $\bar{b} = (1/N) \sum_{i=1}^N b_i$ of the individual scattering lengths b_i of the nuclei with $\sigma_{\text{coh}} = 4\pi |\bar{b}|^2$. \bar{b} is named the coherent scattering length of an atom/nucleus. On the contrary σ_{inc} is fundamentally related to the fluctuations of b_i with $\delta b_i = b_i - \bar{b}_i$ and $\sigma_{\text{inc}} = 4\pi |\overline{\delta b}|^2$. The total scattering cross-section of the whole sample (after integrating over all scattering angles and energies) is given by $\sigma_{\text{tot}} = N(\sigma_{\text{coh}} + \sigma_{\text{inc}}) = 4\pi N |\bar{b}|^2 = 4\pi \sum_{i=1}^N |b_i|^2$.

These fundamental relationships allow to find the partial incoherent cross-sections of the nuclei of M various types S_k (different isotopes of the same chemical element or chemically different elements) in a mixture of various atom types, with specific amounts of atoms N_k , $\sum_{k=1}^M N_k = N$ and concentrations $c_k = N_k/N$, specific coherent scattering lengths $b_{k,c} := \bar{b}_k = (1/N_k) \sum_{i \in S_k} b_i$, and partial coherent,

$\sigma_{k,\text{coh}} = 4\pi |\bar{b}_k|^2$, and incoherent, $\sigma_{k,\text{inc}} = 4\pi |\delta \bar{b}_k|^2$, cross-sections per atom of the specific type k , correspondingly. Here, $|\delta \bar{b}_k|^2 = |\bar{b}_k|^2 - |\bar{b}_k|^2$. In this case, the total scattering cross-section per atom is given by $\sigma_{\text{tot}} = 4\pi |\bar{b}|^2 = 4\pi \sum_k c_k |\bar{b}_k|^2$ and the coherent cross-section equals $\sigma_{\text{coh}} = 4\pi |\bar{b}|^2$ with $\bar{b} = \sum_{k=1}^M c_k \bar{b}_k$. Their difference yields the incoherent cross-section per atom [6, 16]

$$\begin{aligned} \sigma_{\text{inc}} &= \sum_{k=1}^M c_k \sigma_{k,\text{inc}} + 2\pi \sum_{i=1}^M \sum_{j=1}^M c_i c_j |\bar{b}_i - \bar{b}_j|^2 \\ &= \sum_{k=1}^M c_k \tilde{\sigma}_{k,\text{inc}} \end{aligned} \quad (2)$$

with the renormalized incoherent cross-sections

$$\tilde{\sigma}_{k,\text{inc}} = \sigma_{k,\text{inc}} + 2\pi \sum_{j=1}^M c_j |\bar{b}_k - \bar{b}_j|^2 \quad (3)$$

of the components k . This latter renormalization is usually very important for the mixture of isotopes of the same element, where it is named isotope incoherence. Its neglect can lead to entirely wrong results. For example, natural nickel consists mostly of the mixture of two isotopes ^{58}Ni and ^{60}Ni , both having zero incoherent cross-sections. However, the incoherent cross-section of natural nickel is pretty large, $\sigma_{\text{Ni},\text{inc}} = 5.2$ barn, owing to the isotope incoherence.

An akin phenomenon is called chemical incoherence [6] but is usually neglected when applied to a mixture of chemical elements. Whether or not its neglect is correct must be clarified in any concrete case. For example, in a mixture (alloy) of natural gallium (consisting of two isotopes) and either ^{58}Ni or ^{60}Ni , chemical incoherence clearly cannot be neglected. As a striking example of chemical incoherence, let us consider an alloy $\text{Al}_{1-x}\text{Ni}_x$ of aluminium, Al, and ^{58}Ni . ^{58}Ni has zero incoherent scattering cross-section, $\sigma_{\text{Ni},\text{inc}} = 0$, and for aluminium it is tiny, $\sigma_{\text{Al},\text{inc}} = 0.0086$ barn [16]. However, the atoms in the alloy will have, on average, an appreciable $\sigma_{\text{inc}} = (1-x)\sigma_{\text{Al},\text{inc}} + 4\pi x(1-x)|b_{\text{Al},\text{c}} - b_{\text{Ni},\text{c}}|^2 = 0.0086(1-x) + 15.07 \cdot x(1-x)$ barn because the difference of $b_{\text{Al},\text{c}} = 3.449$ fm, and $b_{\text{Ni},\text{c}} = 14.4$ fm for ^{58}Ni [16] is quite significant. It reaches 3.772 barn at $x = 0.5$. Indeed, experiments show that such alloys scatter incoherently in a very profound manner, cf figure 5.1 in [17].

To avoid dealing further with chemical incoherence in this paper, we investigate an alloy of natural gallium and natural nickel at a small concentration of Ni. For Ga, $\sigma_{\text{Ga},\text{inc}} = 0.16$ barn and $b_{\text{Ga},\text{c}} = 7.288$ fm [16]. For natural Ni, $b_{\text{Ni},\text{c}} = 10.3$ fm. Thus, at atomic concentrations $c_{\text{Ga}} = 0.98$ and $c_{\text{Ni}} = 0.02$, we obtain $\tilde{\sigma}_{\text{Ga},\text{inc}} \approx 0.17$ barn and $\tilde{\sigma}_{\text{Ni},\text{inc}} \approx 5.76$ barn. Hence, following equation (2), $\sigma_{\text{inc}} \approx 0.28$ barn, which is less than 10% larger than 0.26 barn achieved when neglecting chemical incoherence. The relative contributions of gallium, $w_{\text{Ga}} = c_{\text{Ga}}\sigma_{\text{Ga},\text{inc}}/\sigma_{\text{inc}}$, and nickel, $w_{\text{Ni}} = c_{\text{Ni}}\sigma_{\text{Ni},\text{inc}}/\sigma_{\text{inc}}$, in the incoherent scattering process are almost not changed upon

renormalization: $w_{\text{Ga}} \approx 0.60$ before, and $\tilde{w}_{\text{Ga}} \approx 0.59$ after the renormalization. Therefore, we neglect chemical incoherence in this paper.

Furthermore, $S_\alpha(\vec{Q}, \omega)$ in equation (1) denotes the Fourier-transform [5–7], $S_\alpha(\vec{Q}, \omega) = (1/2\pi\hbar) \times \int_{-\infty}^{\infty} I_\alpha(\vec{Q}, t) e^{-i\omega t} dt$, of the coherent ($\alpha = \text{coh}$) or incoherent ($\alpha = \text{inc}$) intermediate scattering function (ISF), respectively. The coherent ISF is related to the double sum, $I_{\text{coh}}(\vec{Q}, t) = (1/N) \sum_{i=1}^N \sum_{j=1}^N \langle e^{-i\vec{Q}\vec{R}_i(0)} e^{i\vec{Q}\vec{R}_j(t)} \rangle$, where $\vec{R}_i(t)$ is the time-dependent location operator of atom i and $\langle \dots \rangle$ denotes a quantum-mechanical statistical averaging. Given this mathematical structure, in the case of a multi-component mixture, the coherent dynamical spectrum part, $\sigma_{\text{coh}} S_{\text{coh}}(\vec{Q}, \omega)$, is split into a sum of ‘pure’ components which correspond to the summation indices in the above double sum running only over the subset of one species, and also the cross-terms where one summation index i runs over one species with $i \in S_k$ while another index j runs over a different species with $j \in S_{k' \neq k}$. Evaluation of the corresponding sums allows finding ISFs from the particle trajectories obtained, e.g. with the help of MD simulations as it is implemented, e.g. in the nMOLDYN3 software [18–20]. However, the incoherent ISF corresponds to a single sum $I_{\text{inc}}(\vec{Q}, t) = (1/N) \sum_{i=1}^N \langle e^{-i\vec{Q}\vec{R}_i(0)} e^{i\vec{Q}\vec{R}_i(t)} \rangle$. Hence, there cannot be cross-terms in the case of multi-component mixtures. It compels that the incoherent contribution in equation (1) must be decomposed as

$$\sigma_{\text{inc}} S_{\text{inc}}(\vec{Q}, \omega) = \sum_{k=1}^M c_k \tilde{\sigma}_{k,\text{inc}} S_{k,\text{inc}}(\vec{Q}, \omega) \quad (4)$$

with the renormalized $\tilde{\sigma}_{k,\text{inc}}$ given in equation (3). Indeed, integration of equation (4) over all \vec{Q} and ω must yield the total incoherent cross-section per one atom in equation (2). $S_{k,\text{inc}}(\vec{Q}, \omega)$ is related via the corresponding Fourier-transform to the above single sum with $i \in S_k$ and $N \rightarrow N_k$. Unfortunately, this important renormalization in equations (3), (4) is omitted for a mixture of different chemical elements in most textbooks [6, 7] and software packages [18, 20] devoted to QENS although the importance of isotope incoherence [5–7] and chemical incoherence [6] is well recognized. It must be recalled here that equation (1) is derived based on the assumption that scattering length b_j and the nuclei positions are not correlated [5–7]. Our way to take chemical incoherence into account by the renormalization (equation (3)) of incoherent cross-sections is a consistency condition within a theory based on this fundamental assumption.

Experimentally, $\frac{\partial^2 \sigma}{\partial \Omega \partial E'}$ is measured, e.g. in TOF experiments. In the case of liquids, including liquid metals, it allows finding integral $S_{\text{inc}}(\vec{Q}, \omega)$ at sufficiently small Q -values, where contribution of the coherent scattering spectrum is minor and can be included into a small background spectrum $b(Q, \omega)$. The diffusion of atoms is reflected experimentally

within a diffusional approximation by a Lorentzian incoherent dynamical spectrum function [5–7, 10, 13, 14]

$$S_{\text{obs}}(Q, \omega) = \frac{a(Q)}{\pi} \frac{\Gamma(Q)}{\hbar^2 (\omega - \omega_0)^2 + \Gamma^2(Q)} \otimes R(Q, \omega) + b(Q, \omega) \quad (5)$$

with a spectral half-width $\Gamma(Q)$. The collected experimental spectra $S_{\text{exp}}(Q_i, \omega)$ are convoluted with the energy resolution function of the spectrometer $R(Q, \omega)$ [10, 13, 14]. Moreover, a background function $b(Q, \omega) = b_0(Q) - b_1(Q)\omega$ (in one of the simplest approximations) is added. It reflects a scattering background, which mostly is not originated from the scattering of the sample, and, nevertheless, must be taken into account upon data evaluation. While doing data analysis in the presence of a distinct background bias, $b_1 \neq 0$, one should also generally shift the Lorentzian spectrum by some $\omega_0 \neq 0$, cf equation (5). In such a setting, b_0, b_1 and ω_0 are just some fitting parameters without physical significance. For several TOF neutron spectrometers, the energy resolution function can be approximated by a Gaussian, $R(Q, \omega) \approx (1/\sqrt{2\pi\epsilon^2})e^{-(\hbar\omega)^2/(2\epsilon^2)}$.

For data reduction, the data analysis software FRIDA [21] was used. First, the raw data were corrected for the detector efficiency and the elastic time channel was determined from the vanadium reference data. Subsequently, such collected experimental $S_{\text{exp}}(2\theta, \text{TOF})$ data were further corrected for background, transformed to Q and ω scales, and de-convoluted with the experimentally found resolution function $R(Q, \omega)$ of the spectrometer to achieve the final set of experimental scattering spectra $S_{\text{obs}}(Q_i, \omega)$ for $Q_i \in \{0.4 \text{ \AA}^{-1}, 0.5 \text{ \AA}^{-1}, \dots\}$. Finally, the Lorentzian of the diffusion model, cf equation (5), was fitted to $S_{\text{exp}}(Q_i, \omega)$ by a non-linear least squares algorithm. From this procedure, both spectral width $\Gamma(Q_i)$ and $a(Q_i)$, which represents an experimental weight factor proportional to σ_{inc} , can be determined. In this diffusional approximation, $\Gamma(Q) = \hbar D Q^2$, where D denotes the diffusion coefficient [5]. The corresponding $I(Q, t)$ is a single-exponential, $I(Q, t) = \exp(-\Gamma t/\hbar)$ (after normalizing on $I(Q, 0)$). This data evaluation approach has recently been applied successfully to many liquid metals and liquid alloys [8–10, 13, 14].

Another data evaluation approach is based on $I_{\text{obs}}(Q, t)$ determined by fast Fourier transformation of $S_{\text{obs}}(Q, \omega)$ after background subtraction. $I_{\text{obs}}(Q, t)$ is divided by $I_d(Q, t)$ which represents the inverse Fourier-transform of the experimental resolution function of the spectrometer $R_{\text{exp}}(Q, \omega)$ and subsequently normalized to achieve $I_{\text{exp}}(Q, t)$ such that $I_{\text{exp}}(Q, 0) = 1$. $I_{\text{exp}}(Q, t)$ is fitted by a single exponential for the different Q -values. The diffusion coefficient is calculated from a linear fit to the achieved $\Gamma(Q^2)$ data as $\Gamma(Q) = \hbar D Q^2$. The whole procedure has also been performed using the FRIDA program [21].

For multi-component systems, like liquid alloys, diffusion coefficients of different atoms can be very different. In this case, $S_{\text{exp}}(Q, \omega)$ is expected to be a sum of Lorentzians reflecting the diffusional contributions of the different components.

Accordingly, $I_{\text{exp}}(Q, t)$ is expected to be multi-exponential. In particular, it is expected to be bi-exponential in the case of $\text{Ga}_x\text{Ni}_{1-x}$ alloys. However, when the diffusion coefficients of components, D_k , are similar, approximately a single-exponential relaxation will be observed, and scattering spectra will be well approximated by a single Lorentzian. It makes it especially difficult to find particular D_k -values from the experiments. However, within this approximation an effective integral diffusion coefficient observed by QENS for two major chemical components can be formulated as follows:

$$D = w_1 D_1 + w_2 D_2, \quad (6)$$

where $w_k = c_k \sigma_{k, \text{inc}} / [c_1 \sigma_{1, \text{inc}} + c_2 \sigma_{2, \text{inc}}]$, $k = 1, 2$. This formula will be used to compare the results of MD simulations, where individual D_k are found, with experiments providing the integral QENS-value D within the discussed approximations.

3. Experimental

QENS experiments were conducted at the direct geometry TOF neutron spectrometer TOFTOF [22] at the Heinz Maier-Leibnitz neutron source (FRM II) in Garching, Germany, as well as at the Xtof spectrometer FOCUS [23] at SINQ of the Paul Scherrer Institute in Villigen, Switzerland.

For the TOFTOF spectrometer, an incident neutron wavelength of 10 \AA was used coupled with a chopper speed of 3000 rpm and leading to a Q range between 0.1 \AA^{-1} and 1.2 \AA^{-1} and an energy resolution of $\sim 50 \text{ \mu eV}$ (FWHM). At FOCUS, an incident neutron wavelength of 4.4 \AA was chosen using a PG002 monochromator. This setup provided a Q range between 0.4 \AA^{-1} and 2.5 \AA^{-1} with an energy resolution of $\sim 150 \text{ \mu eV}$ (FWHM).

The samples were measured inside custom-made hollow cylindrical Al_2O_3 containers with a wall thickness of 0.5 mm and an inner diameter of 10 mm filled to a height of 40 mm with the sample. Liquid gallium samples, produced from Gallium pellets of 99.9999 % purity (Alfa Aesar), were measured at TOFTOF at temperatures of 340 K, 360 K, 380 K, 400 K, and 420 K, for 1 h and 1.5 h, respectively. Measurements at FOCUS were carried out at temperatures of 473, 823, 1073, and 1273 K, for 3 h each. The $\text{Ga}_{0.98}\text{Ni}_{0.02}$ alloy was produced dissolving 99.99% pure Ni wire (MaTeck) into liquid Ga (99.9999 %, Alfa Aesar). A heat gun was used to maintain the alloy in its liquid state while transporting the samples from the preparation laboratory to the spectrometer. The $\text{Ga}_{0.98}\text{Ni}_{0.02}$ sample was measured at 823 K, 1073 K, and 1273 K, for 3 h. For a background measurement an empty alumina container was measured at 360 K at TOFTOF and at 823 K, 1073 K, and 1273 K at FOCUS. To determine the energy resolution and also to correct for detector efficiency and sample-detector-distance deviations, a standard vanadium sample was measured at room temperature at both spectrometers. Experimental raw data are provided on Zenodo [24].

4. MD simulations

The pure Ga and $\text{Ga}_{0.98}\text{Ni}_{0.02}$ alloy liquid metal systems were studied by means of MD simulations. For this, the Vienna *ab-initio* simulation package (VASP) software [25–28] was used. Both genuine *ab-initio* molecular dynamics (AIMD) using DFT and force field MD utilizing the VASP Machine Learning force field (ML-FF) [29–31] were done. The ML-FFs were trained on the fly based on DFT, where the DFT description of the system was replaced gradually by the much faster ML-FF description. For the AIMD simulations and the DFT steps during the ML-FF learnings, the valence electrons were described via a set of plane wave basis functions, combined with the projector augmented wave (PAW) method for the description of the atomic cores [27, 28, 32]. The Ga ($4s^2 4p^1$) and the Ni ($3d^8 4s^2$) PAW potentials were used. For the ML-FF generations, the kinetic energy cutoff was set to 200 eV (pure gallium) and 350 eV ($\text{Ga}_{0.98}\text{Ni}_{0.02}$ alloys), respectively, in order to incorporate possible relaxations of the unit cell during the heating (see below). For the AIMD simulations of pure Ga, the kinetic energy cutoff was set to 150 eV. Exchange-correlation effects were treated with the exchange correlation functional of Perdew *et al* [33]. A Gamma-containing $2 \times 2 \times 2$ *k*-point mesh was chosen for sampling the Brillouin zone in all cases. Electronic states were always smeared with the first-order Methfessel–Paxton scheme and a broadening of 0.2 eV [34].

For the generation of the ML-FFs within VASP, we proceed as follows. A NpT trajectory was sampled by using the Parinello–Rahman barostat [35, 36] and the Nose–Hoover thermostat [37–39]. No external pressure was applied. The shape of the cubic unit cells was kept by setting constraints with the ICONST file, only uniform volume relaxations were allowed. For pure Ga, 343 Ga atoms were placed in a cubic unit cell on a $7 \times 7 \times 7$ grid. For $\text{Ga}_{0.98}\text{Ni}_{0.02}$, 7 Ni atoms were placed by a home-made script in the largest hole positions of a pre-equilibrated cell with 343 Ga atoms. During the learning, the systems were heated up linearly from 50 K to 1650 K during a span of 700 000 MD steps (pure Ga) and from 500 K to 1700 K during a span of 530 000 MD steps ($\text{Ga}_{0.98}\text{Ni}_{0.02}$). For pure Ga, the time step was set to 5 fs, for $\text{Ga}_{0.98}\text{Ni}_{0.02}$, the time step was set to 10 fs below 1000 K and to 5 fs above 1000 K. Radial and angular descriptor cutoffs were set to 5 Å (pure Ga) and 7 Å ($\text{Ga}_{0.98}\text{Ni}_{0.02}$). The number of radial and angular basis functions was raised during the learning to 15 for both systems, a subsequent refit was done to improve the ML-FF performance. During the learning, 818 DFT reference configurations were collected for pure Ga and 1820 reference configurations were collected for $\text{Ga}_{0.98}\text{Ni}_{0.02}$.

After generation of the ML-FFs, diffusion coefficients of both systems were obtained by averaging over several simulation runs. For pure Ga, 10 ML-FF trajectories containing 343 atoms were ran at 340 K, 360 K, 380 K, 400 K, 420 K, 473 K, 823 K, 1073 K, and 1273 K for 35 000 MD steps of 2 ps length, respectively, where the first 5000 MD steps were always discarded, serving as initial equilibration, resulting in trajectories of 60 ps length each, and a total simulation time of 3.24 ns. The ML-FF trajectories were simulated within the NVT ensemble,

initial cubic box sizes were set based on experimental Ga densities [40], cf table A1 in appendix. For $\text{Ga}_{0.98}\text{Ni}_{0.02}$, 10 ML-FF trajectories were simulated at each temperature as well (823 K, 1073 K and 1273 K). To get better-converged diffusion coefficients for the scarce Ni atoms, larger unit cells were set up, containing 980 Ga and 20 Ni atoms each, which were initialized by placing the Ga and Ni atoms by chance on a $10 \times 10 \times 10$ regular cubic grid in the simulation box of some initial box size, cf figure 1 (a) of the supplementary material [41]. Since no experimental densities were available for those alloy systems, NpT trajectories were simulated, starting at densities near pure Ga, which set the initial box size. The external pressure was set to 0 bar, corresponding to the experimental conditions. The time step was set to 1 fs, resulting in 30 ps simulation time per trajectory, with an additional 5 ps equilibration at the beginning of each trajectory. During equilibration simulation, boxes expanded to an equilibrium size, as illustrated in figure 1 (b) of [41]. In order to test the possible effect of external pressure, the samplings at 1073 K were repeated with 1 bar external pressure applied.

For additional verification of the ML-FF simulations, AIMD trajectories of pure Ga were ran. Since those are significantly more expensive than ML-FF samplings, smaller unit cells, containing 216 Ga atoms each, were set up at the experimental densities. 5 instead of 10 NVT trajectories were simulated at four significant temperatures: 340 K, 420 K, 823 K, and 1273 K. The time step was set to 4 fs, 10 000 MD steps were simulated for each trajectory, from which the last 8750 (35 ps) were used for evaluation.

The AIMD and ML-FF simulations were evaluated with the nMOLDYN3 program package [18–20], which focuses on neutron-scattering oriented analysis of MD simulations and can calculate a whole range of observables from a given MD trajectory file. The corresponding MD trajectory files are provided on Zenodo [24].

In the case of pure Ga the diffusion coefficients were calculated from the mean-square displacement (MSD) of the atoms

$$\Delta^2(t) = \frac{1}{N} \sum_{i=1}^N |\vec{R}_i(t) - \vec{R}_i(0)|^2. \quad (7)$$

In the case of an alloy the summation runs over the atoms of a particular element (Ga or Ni) with N adjusted correspondingly. It allows finding specific diffusion coefficients D_{Ga} and D_{Ni} , respectively. After this, an integral diffusion coefficient to compare with the QENS experiments was found as $D = w_{\text{Ga}}D_{\text{Ga}} + w_{\text{Ni}}D_{\text{Ni}}$ following equation (6). Theoretically, the diffusion coefficient can be found from the MSD as

$$D = \lim_{t \rightarrow \infty} \frac{\Delta^2(t)}{6t}. \quad (8)$$

In practice, it was calculated by summing up the MSDs of all atoms between the first (after equilibration) and the last time steps of the respective trajectory. After obtaining the diffusion coefficients for each trajectory by equation (8), their averages and standard deviations for a certain temperature were calculated.

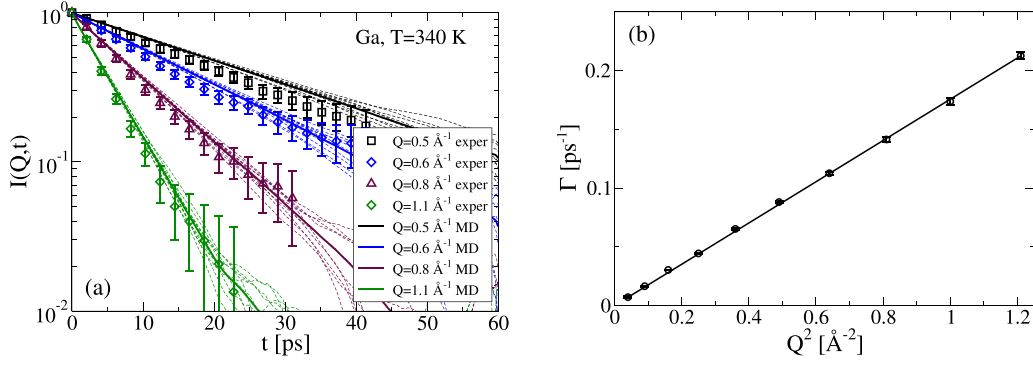


Figure 1. (a) Incoherent intermediate scattering functions versus time for pure liquid gallium at $T = 340$ K for several wave vector values Q given in the legend. Experimental results obtained by experiments at the TOFTOF spectrometer are indicated by symbols. The corresponding results from MD simulations (cf text) are indicated by thin dashed lines for ten different ML-FF MD simulation runs. The ISFs were calculated from the trajectories using nMOLDYN3 software [18–20]. The averaged ISFs are represented by thick solid lines. The experimental and numerical simulation data essentially agree within the statistical errors. (b) Visual representation of the relaxation rate $\Gamma(Q)$ of the experimental $I(Q, t)$ in part (a) as a function of Q^2 (symbols). From the slope of the linear fit to the data the diffusion coefficient D_{Ga} can be calculated. The values of D_{Ga} are listed in table 1 and visualized in figure 2 for different temperatures.

5. Results and discussion

5.1. Pure liquid gallium

QENS experiments and MD simulations were performed on natural liquid gallium (a mixture of two isotopes) at different temperatures. Initially, experiments were performed at the TOFTOF spectrometer of the Heinz Maier-Leibnitz neutron source (FRM II) in Garching for $T = 340$ K, 360 K, 380 K, 400 K, and 420 K. This spectrometer has nearly Gaussian energy resolution function with $\epsilon \approx 21 \mu\text{eV}$ (and FWHM $w = 2\sqrt{2\ln 2}\epsilon \approx 49.4 \mu\text{eV}$). Some experimental results on the decay of the ISF are shown (with symbols) for $T = 340$ K and several values of Q in figure 1(a). The exponential fits of the data yield a relaxation rate $\Gamma(Q)$ which is depicted with symbols as a function of Q^2 in figure 1(b). The linear fit of this latter dependency comes through all experimental data points within tiny, less than 1% error bars. It yields the diffusion coefficients of gallium given in table 1 and figure 2 (black circles) for different temperatures. The diffusion coefficient of Ga was also derived for two of these temperatures from AIMD simulations, as well as ML-FF-MD simulations with the results given in table 1 and figure 2 (red asterisks for AIMD and blue diamonds for ML-FF-MD). AIMD and ML-FF-MD well agree within statistical errors at $T = 340$ K and $T = 420$ K. However, ML-FF-MD somewhat overestimates the diffusion coefficient compared with AIMD, which leads to a partial error cancellation with respect to the experimental values below 500 K. It is a general feature valid also for other temperatures in our simulations.

The agreement between theoretical and experimental results is also clearly present. Importantly, ML-FF-MD agrees within error bars for four temperatures out of five with the experimental results, and for $T = 340$ K, a discrepancy is small, less than 6% in the mean values. The agreement between AIMD and experiment is slightly lower. Nevertheless, at $T = 420$ K simulations and experiments agree within the error bars, and at $T = 340$ K the discrepancy

between the mean values is less than 12%. The small deviations between ML-FF-MD and AIMD indicate ML-FF-MD as a method of choice in further studies.

ISFs were also obtained from ML-FF-MD simulations using nMOLDYN3. The results presented in figure 1(a) for ten MD realizations and their average at 340 K and four values of Q , namely, 0.5 \AA^{-1} , 0.6 \AA^{-1} , 0.8 \AA^{-1} , and 1.1 \AA^{-1} mostly agree with the experimental results within the error bars. This confirms that theory and experiment agree well.

Measurements for higher temperatures, namely, 473 K, 823 K, 1073 K, and 1273 K were performed at the neutron spectrometer FOCUS at the Paul Scherrer Institute, Switzerland. It also possesses a nearly Gaussian energy resolution function with somewhat larger $\epsilon \approx 64.3 \mu\text{eV}$ (FWHM $w \approx 151.4 \mu\text{eV}$). In this case, the calculation of the ISFs from experimental data was not possible due to the limited counting statistics. However, the experimental scattering functions $S(Q, \omega)$ could be calculated from the raw data and are visualized for $T = 823$ K in figure 3(a) for two values of Q including the plots of the corresponding Lorentzian fits convolved with the experimental resolution function $R(Q, \omega)$ of the spectrometer, and the background intensity present. The corresponding plots for two additional larger values of Q are provided in figure 2(a) of supplementary material [41]. The half-width $\Gamma(Q)$ of the Lorentzians is plotted as a function of Q^2 in figure 3(b) together with a linear fit. The values of the extracted diffusion coefficients are included in table 1 and plotted with black circles in figure 2. Due to the reduced counting statistics and a significantly broadened signal at the higher temperatures, the experimental errors are larger compared to the TOFTOF data. Hence, some discrepancies with the theoretical MD results (not within error bars) become apparent.

At $T = 823$ K the discrepancy is about 12 % of the mean values. Despite this, the agreement with the AIMD result is almost present within error bars (cf table 1). However, for two highest temperatures, the discrepancy increases to 21–32% and becomes distinct beyond error bars. Nevertheless, for $T = 473$ K the numerical theory and the data from the

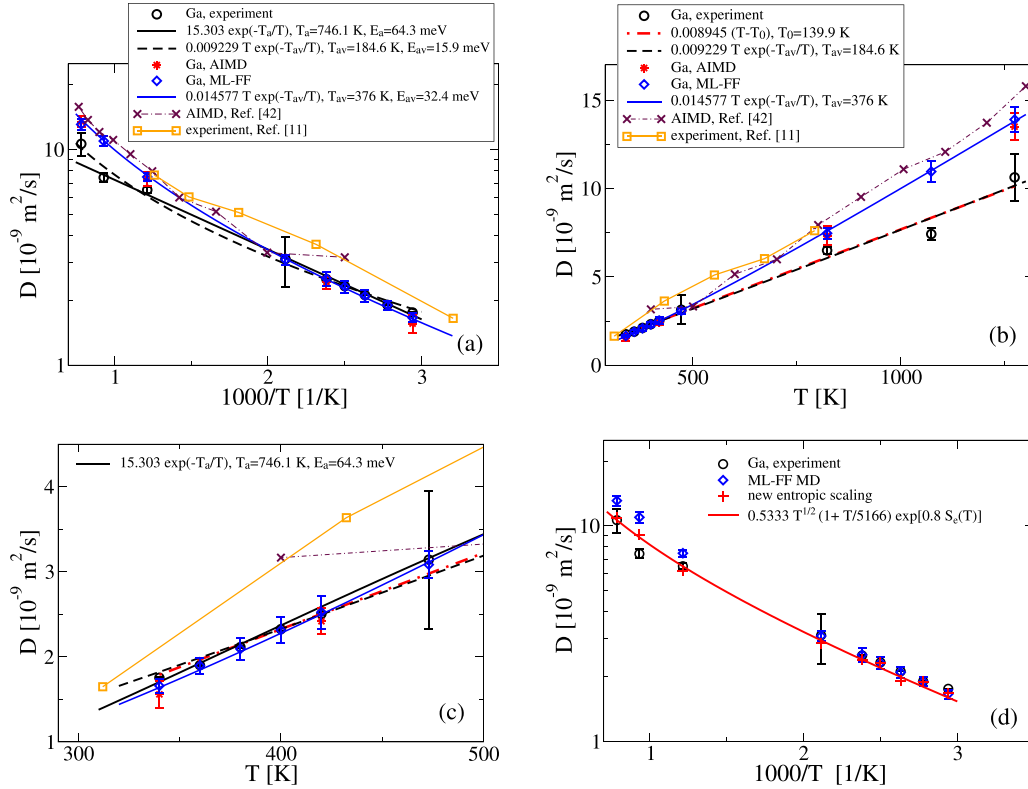


Figure 2. (a) Arrhenius plot for the diffusion coefficient of liquid gallium. Experimental values (black circles) agree well with both *ab initio* (red asterisks) and classical MD simulation results using machine-learning force fields (blue diamonds) for $T < 500$ K. Black solid and dashed lines represent the best Arrhenius fit, cf equation (9), and the fit with the Einstein–Stokes dependence, cf equation (12), of the experimental data. Notice that the effective viscosity activation energy E_{av} in the later fit is about four times smaller than E_a . Blue solid line presents best fit of the numerical MD results with equation (12). (b) Linear plot of the data presented in subfigure (a). The linear fit (red dash-point line), $D(T) \approx k_B(T - T_0)\mu_0$, describes the experimental data well. This already follows from the expansion of the Einstein–Stokes temperature dependence for a small viscosity activation energy $E_{av} = k_B T_{av} \ll k_B T$ and using a fitting value T_0 instead of T_{av} . It is also shown in the plot. Orange squares represent experimental data extracted from figure 3 in [11], and maroon crosses reproduce AIMD data extracted from figure 7(a) in [42] using Engauge-Digitizer [43]. (c) The same as (b), but restricted to $T < 500$ K, with the fit to the experimental values from part (a) added. (d) Arrhenius plot with experimental and ML-FF MD results from (a) compared against the numerical results (red crosses) stemming from the new entropic scaling in equation (11) and obtained by evaluation and interpretation of MD results in terms of the excess entropy, see tables 1 and 2 in [41]. The red line comprises the product of two terms. The first is the exponential entropic factor analytically described by equation (10) with fitting parameters $S_0 = 0.5057$ and $T_s = 625.3$ K, cf figure 5(b) of [41]. The second is the prefactor function from figure 6(a) of [41].

Table 1. Diffusion coefficient for Ga (in $10^{-9} \text{ m}^2 \text{ s}^{-1}$, including standard deviation) at different temperatures.

T , K	$D_{\text{Ga, experiment}}$	$D_{\text{Ga, AIMD}}$	$D_{\text{Ga, ML-FF}}$
340	1.755 ± 0.010	1.560 ± 0.155	1.660 ± 0.080
360	1.903 ± 0.013		1.898 ± 0.094
380	2.115 ± 0.014		2.094 ± 0.127
400	2.326 ± 0.016		2.314 ± 0.151
420	2.505 ± 0.017	2.419 ± 0.153	2.525 ± 0.195
473	3.108 ± 0.810		3.083 ± 0.162
823	6.500 ± 0.205	7.332 ± 0.537	7.470 ± 0.298
1073	7.425 ± 0.355		10.961 ± 0.612
1273	10.634 ± 1.335	13.502 ± 0.773	13.907 ± 0.719

experiment at FOCUS still agree within the statistical errors. Overall it can be concluded that a discrepancy between the experimental and simulation data appears at temperatures

above 500 K (cf figure 2). Its origin could not be clarified yet. Notice that at $T = 823$ K and $T = 1273$ K AIMD was closer to experiment than ML-FF-MD which yielded diffusion coefficients up to 6% larger than achieved from AIMD.

It is worth also mentioning that for the largest diffusion coefficients in table 1, e.g. at $T = 1273$ K one can question the standard way of how they were obtained because the diffusional spread of particles becomes at the end of simulation of the box size. However, the alternative way of calculating diffusion coefficient as integral of stationary velocity autocorrelation function [5, 19], which decays on a much shorter time scale of merely few picoseconds, yielded (AIMD) $D = 13.551 \cdot 10^{-9} \text{ m}^2 \text{ s}^{-1}$ at $T = 1273$ K, see section 3 and figure 4 in [41]. It agrees very well with $D = 13.502 \cdot 10^{-9} \text{ m}^2 \text{ s}^{-1}$ in table 1. Hence, smaller MD diffusion coefficients in this table are also beyond doubt. Thus, we trust the MD results for three largest temperatures because the experimental results in those cases have poorer statistics than for other temperatures. To

improve it one needs to dramatically increase the time duration of the experiment, which would require a separate investigation beyond the present study.

5.2. Temperature dependence of the diffusion coefficient in liquid gallium

The experimental dependence of gallium self-diffusion coefficient scaled logarithmically on the inverse temperature in figure 2(a) can be fitted by a straight line revealing an Arrhenius dependence on temperature

$$D(T) = D_0 e^{-E_a/(k_B T)}, \quad (9)$$

with $E_a = k_B T_a \approx 64.3$ meV, and $D_0 \approx 15.303 \cdot 10^{-9} \text{ m}^2 \text{ s}^{-1}$. This fit also agrees very well with the MD results at temperatures below 500 K. The physical origin of this fit for liquids can be rationalized with a scaling theory based on the excess entropy $S_e(T, n)$ being the difference between the entropy per one particle of the condensed system considered and the corresponding ideal gas at the same temperature T and number density n [44–50]. Within the corresponding scaling theory [44–50], $D(T)$ exponentially depends on S_e , $D(T) = D_0(T) A \exp[\alpha S_e(T)]$, with α being a constant of the order of unity, and A is some other numerical constant. In the Rosenfeld theory $\alpha = 0.8$ and $A = 0.6$ [45, 47], whereas in the Dzugutov theory $\alpha = 1$ and $A = 0.049$ [46, 48]. These two variants of scaling theory essentially differ in prefactors $D_0(T)$, cf [41], section 4, for some detail. In the Rosenfeld scaling, $D_0(T) = v_T n^{-1/3}$ is determined by the product of thermal velocity, $v_T = \sqrt{k_B T/m}$, where m is the mass of particle, and the mean distance $n^{-1/3}$ between particles. In the Dzugutov scaling, $D_0(T) = \sigma^2 \Gamma_E$, where σ is the position of the maximum of the radial (pair) distribution function $g(r)$, and $\Gamma_E = 4\sqrt{\pi} \sigma^2 g(\sigma) n v_T$ is the Enskog collision frequency between hard spheres of diameter σ in the gas of density n [46, 51]. The Dzugutov scaling was also derived from a mode-coupling theory [50] showing that $D_0(T) = D_0$ is not temperature-dependent; see also table 2 and figure 6(a) in [41] along with the corresponding discussion. Together with the assumed temperature dependence (S_e is scaled here in the units of k_B)

$$S_e = -S_0 - T_s/T. \quad (10)$$

It justifies equation (9) with $E_a = k_B T_s$, and the renormalized $D_0 \rightarrow D_0 A \exp(-S_0)$. Astoundingly, the Dzugutov scaling was confirmed in many liquid metals, Pb, Cu, Ag, Au, Cu, Pd, Pt, including Ni, as well as several alloys, Ni₃Al, AgI, AuPt [46, 49], what makes it especially relevant for our study. However, as we show in [41] based on our MD results, it fails for liquid gallium, which is also an important result. Namely, it overestimates the diffusion coefficient by a factor of four. After a corresponding rescaling by this factor, it does fit well our results for $T < 500$ K with $E_a = k_B T_s = 53.9$ meV, cf figure 6(b) in [41]. However, it fails for $T > 500$ K to describe both experimental and theoretical results. Nevertheless, it is important

because of the physical insight it provides. Moreover, the corresponding activation energy of 53.9 meV is not much different from our fit value of 64.3 meV. It allows us to fit the results alternatively for $T < 500$ K [41].

Furthermore, the Rosenfeld scaling with $D_0(T) \propto T^{1/2}$ and $E_a = 43.1$ meV [41] also strongly overestimates the Ga diffusion coefficient. However, with the additional factor of 0.35, it fits the experimental data in the whole temperature range. It is much closer to MD simulation results at large temperatures than the rescaled Dzugutov scaling, cf figure 6(b) in [41]. One should notice in this respect that having a power-law temperature dependence of the prefactor function $D(T)$ instead of being constant while fitting the same data corresponds to a numerically different activation energy. In a comparison of the two discussed variants of the scaling theory, the difference is accounted for by the factor $\alpha = 0.8$, even though in both variants, the physical origin of this activation energy is due to the inverse temperature dependence of the excess entropy in equation (10). Bastea suggested one more scaling [52]. Like one of Rosenfeld, it has $\alpha = 0.8$; however, the prefactor function comprises of Boltzmann diffusion coefficient, $D_B = (3\sqrt{\pi}/8) l_B v_T$, where $l_B = 1/(\pi n \sigma^2)$ is the Clausius-Boltzmann mean free path length in the gas of hard spheres with diameter σ [51], multiplied with $g(\sigma)$. It agrees with one of Dzugutov at large $-S_e > 3$ [52]; however, it deviates from it at smaller $-S_e$. Like Rosenfeld scaling, it also overestimates the diffusion coefficient by a factor of three in gallium [41]. As a remedy for this, we propose a new prefactor scaling very similar to one of Bastea by dropping the factor $g(\sigma)$:

$$D(T) = \tilde{A} l_B v_T e^{0.8 S_e(T)}, \quad (11)$$

where $\tilde{A} = 3\sqrt{\pi}/8 \approx 0.6647$. It is very similar at the same time to the Rosenfeld scaling with $l_0 = n^{-1/3}$ being replaced by l_B and $A = 0.6$ with \tilde{A} . Our new prefactor scaling agrees well with the experimental results in figure 2(d). It has the same activation energy $E_a = 43.1$ meV as in the Rosenfeld scaling. The prefactor has the main \sqrt{T} dependence stemming from v_T . The mean free path l_B is almost constant for $T < 500$ K. However, it increases for $T > 500$ K; see table 1 in [41]. Interestingly, neither $n^{-1/3}$ nor σ as characteristic spatial scales indicate such a change [41]. This behavior correlates with lowering the coordination number of the first coordination shell from 11 to 11.5 at $T < 500$ K to 9.5 at 1273 K, see figure 7 in [41]. It indicates a gradual structural transition in liquid Ga. From a tightly packed liquid resembling a hard sphere system at $T < 500$ K, it becomes less densely packed upon further temperature elevation. It explains the failure of earlier scaling theories for this anomalous liquid, which, like water, becomes heavier upon melting. The failure of known scaling theories for anomalous liquids like water, Si is already well recognized in the literature [44, 49]. From this perspective, their failure for Ga is not that surprising. However, our new scaling dependence in equation (11) works for Ga. In future research, it needs to be clarified whether it will work for other anomalous liquids and correspond to some sufficiently broad universality class as the Rosenfeld and Dzugutov scalings do.

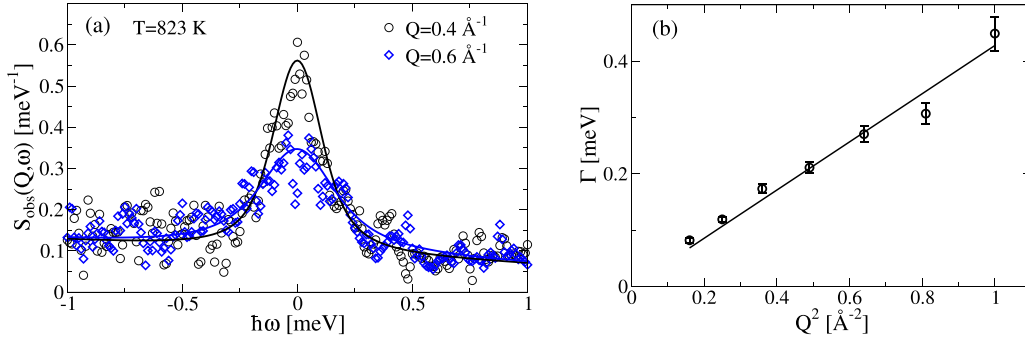


Figure 3. (a) QENS spectra of pure liquid gallium at $T = 823 \text{ K}$ (symbols, FOCUS spectrometer) for two Q -values. The solid lines represent the best fits by a single Lorentzian (cf equation (5)) to the experimental data. (b) $\Gamma(Q)$ of the Lorentzian (symbols) derived from the fits to the experimental data and plotted as a function of Q^2 . The solid line represents the best linear fit to the data.

We would also like to note that pioneering experiments on self-diffusion in natural gallium using radioactive gallium tracer yielded much lower activation energy $E_a = 11.63 \text{ meV}$ with $D_0 = 10.7 \cdot 10^{-9} \text{ m}^2 \text{ s}^{-1}$ and $T_a = 134.95 \text{ K}$ [53]. In the light of our results displaying an excellent agreement of experiment with simulations at $T < 500 \text{ K}$, this old result must be questioned. From a theoretical point of view, once the integral of VACF converges after a few picoseconds to a constant diffusion value, it will characterize diffusion on arbitrarily larger timescales, provided that the liquid remains homogeneous on larger spatial scales. Deviation from the liquid's homogeneity in first experiments might be the reason for the deviation of old results from the correct ones. However, whether it was or not the case is impossible to clarify.

More recent QENS results [11], which were extracted from figure 3 in [11] using Engauge-Digitizer [43], are depicted with orange squares in figures 2(a)–(c). They agree quite closely with our results. Also the reported activation energy of 60 meV [11] is close to the value found in our QENS study. Interestingly, the results of AIMD simulations of Ga diffusion in [42] differ from our AIMD results at lower temperatures but are, nevertheless, closer to our results at temperatures above 500 K . At $T = 673 \text{ K}$ and $T = 793 \text{ K}$, the MD simulation results interpolated by connecting lines appear somewhat closer to the experimental results in [11], which, however, do not agree quantitatively with the MD simulations at lower temperatures, in contrast to our experimental results. Additional MD simulation results were extracted using Engauge-Digitizer [43] from figure 7(a) in [42] and are depicted with maroon crosses in figures 2(a)–(c). From this data, an activation energy of $E_a = 84.1 \text{ meV}$ (8.12 kJ mol^{-1}) was extracted at temperatures below 1000 K [42]. It is significantly larger than the value observed in our simulations. Moreover, the AIMD simulations in [42] exhibit a different even larger activation energy of $E_a = 163.5 \text{ meV}$ ($15.78 \text{ kJ mol}^{-1}$) for temperatures above 1000 K (cf figure 7(a) in [42]). Our MD simulations reveal an essentially smaller activation energy for $T < 500 \text{ K}$, cf figure 2(c). However, the simulations also reveal an increase of the activation energy for $T > 500 \text{ K}$, which does not agree with our experimental data, as it can clearly be seen in figure 2(a).

Alternatively, our experimental data can also be fitted very well by an Einstein-Stokes dependence

$$D(T) = \frac{k_B T}{\eta(T)} = k_B T \mu_0 e^{-E_{av}/(k_B T)}, \quad (12)$$

where it is respected that the diffusion coefficient and the mobility $\mu(T)$ are linked by the fluctuation-dissipation theorem at thermal equilibrium: $D(T) = k_B T \mu(T)$. It is further assumed that the inverse atom mobility $1/\mu(T) = \eta(T)$ or viscous friction coefficient of gallium can be described by the Stokes formula $\eta(T) = 6\pi R \zeta(T)$, where R is the effective hydrodynamic radius of gallium and $\zeta(T)$ denotes the viscosity obeying the Arrhenius dependence $\zeta(T) = \zeta_0 \exp[E_{av}/(k_B T)]$ with the activation energy $E_{av} = k_B T_{av}$. The latter dependence is well established for gallium with $T_{av} = 204.3 \ln(10) = 469.8 \text{ K}$, $E_{av} = k_B T_{av} = 40.5 \text{ meV}$, and $\zeta_0 = 0.3577 \text{ mPa}\cdot\text{s}$ for T between 303 K and 800 K [40]. For a small activation energy ($E_{av}/(k_B T) \ll 1$), equation (12) yields

$$D(T) \approx k_B \mu_0 (T - T_{av}). \quad (13)$$

Using a free fitting value T_0 for T_{av} in equation (13) and another fitting value of μ_0 is expected to provide better results.

However, the fit with equation (12) yields much smaller values for $T_{av} = 184.6 \text{ K}$ and $E_{av} = k_B T_{av} = 15.9 \text{ meV}$, cf figure 2(a). Interestingly, these values are closer to the fitting values in [53] where equation (9) has been used. Our fitting value μ_0 is $\mu_0 = 6.686 \cdot 10^{11} \text{ s kg}^{-1}$. Using the Stokes formula with the above experimental value for ζ_0 yields $R = 2.22 \text{ \AA}$ which is only about 19% larger than the van-der-Waals radius of gallium $R_{vdW} = 1.87 \text{ \AA}$ and is, therefore, a reasonable estimate.

Strikingly enough, our MD simulation results are excellently fitted by equation (12) (cf solid blue line in figure 2(a)–(c)) at all temperatures with $T_{av} = 376 \text{ K}$ and $E_{av} = k_B T_{av} = 32.4 \text{ meV}$ which are not that far from the experimental values given in [40] and $\mu_0 = 1.056 \cdot 10^{12} \text{ s kg}^{-1}$. This fit should be preferred over the fit with equation (9) on general theoretical grounds, and in the view of the failure of the Dzugutov scaling theory justifying this fitting dependence in equation (9) for many other melted metals, as discussed above. Using the

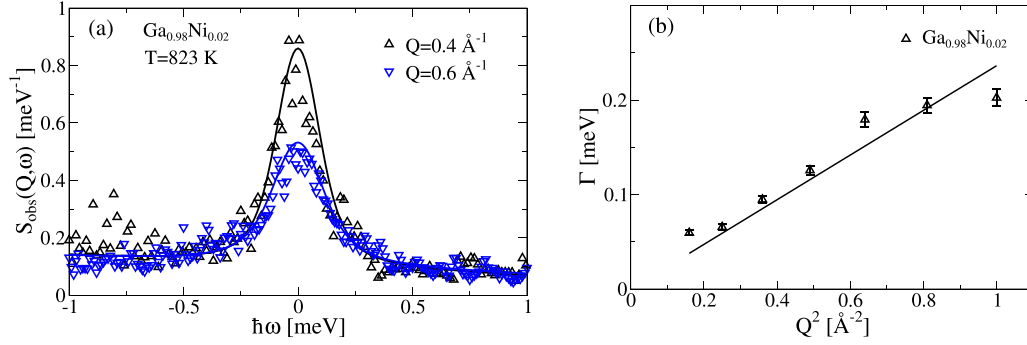


Figure 4. (a) QENS spectra of the liquid gallium-nickel alloy $\text{Ga}_{0.98}\text{Ni}_{0.02}$ at $T = 823$ K (symbols, FOCUS spectrometer) for two Q -values. The solid lines represent the best fits by a single Lorentzian, cf equation (5), to the experimental data. (b) Half-width $\Gamma(Q)$ of the Lorentzian (symbols) derived from the fits to the experimental data is plotted as a function of Q^2 . The solid line represents the best linear fit to the data.

Table 2. Diffusion coefficients for $\text{Ga}_{0.98}\text{Ni}_{0.02}$ (in units of $10^{-9}\text{m}^2\text{s}^{-1}$, including standard deviation) at different temperatures.

T (K)	D_{Ga} , MD	D_{Ni} , MD	D , theory	D , experiment
823	3.881 ± 0.126	2.202 ± 0.343	3.209 ± 0.157	3.602 ± 0.719
1073	5.905 ± 0.142	3.762 ± 0.824	5.047 ± 0.340	4.639 ± 0.306
1273	7.381 ± 0.283	5.162 ± 1.250	6.493 ± 0.528	5.759 ± 0.604

experimental value of ζ_0 , it yields $R = 1.41 \text{ \AA}$, which is close to $\sigma/2$ in table 1 [41], which varies with temperature very weakly. This striking correspondence provides an additional justification for this fit. The Einstein–Stokes formula with a constant $R \approx \sigma/2$ combined with an exponential dependence of the gallium viscosity on the temperature measured in experiments [40] fully suffices to parameterize and thus explain the MD results on gallium self-diffusion. This physical explanation is a reasonable alternative to one based on the excess entropy scaling and equation (11).

Of course, application of the macroscopic hydrodynamics Stokes formula to atomic diffusion is rather questionable and is not warranted to hold on the microscopic time scale of picoseconds probed by QENS. This was the reason for using equation (9) for initial fits to the data, as it was also done earlier for other liquid metals and alloys [8–10, 13, 14]. However, we stress that a linear fit of experimental results with equation (13) stemming from equation (12) works also remarkably well (cf figure 2(b)) revealing $T_0 = 139.9 \text{ K}$. It cannot be distinguished from the fit with equation (12) by the fit quality. Moreover, our numerical theory data much better comply with equation (12) while avoiding to introduce a temperature-dependent diffusion activation energy.

5.3. Liquid gallium-nickel alloy

The liquid alloy of natural gallium and nickel $\text{Ga}_{0.98}\text{Ni}_{0.02}$ has been studied at the FOCUS spectrometer at three different temperatures of 823 K, 1073 K, and 1273 K. The experimental scattering functions $S(Q, \omega)$ at $T = 823 \text{ K}$ are plotted in figure 4(a) for two Q -values together with the corresponding Lorentzian fits convolved with the energy resolution function of the spectrometer and respecting a background linear intensity, see also figure 2(b) of supplementary material [41]

for two larger values of Q . $\Gamma(Q)$ of the Lorentzian fit is plotted as a function of Q^2 in figure 4(b) together with a linear fit. The integral diffusion coefficients obtained in this way for all temperatures are listed in table 2 and visualized as a function of temperature by blue up-triangles in figure 5. We also performed ML-FF-MD simulations for this alloy at the same temperatures, which yielded theoretical values for diffusion coefficients of gallium and nickel in this alloy separately. They are also given in table 2 and presented in figure 5 by red asterisks (gallium) and magenta diamonds (nickel). We obtained an integral diffusion coefficient from these specific values, to compare it with one measured by QENS. These values are also listed in table 2 and visualized as dark green up-triangles in figure 5. The simulation and experimental results agree within the error bars.

We also checked the influence of pressure on the MD diffusion coefficient upon changing it from 0 to 1 bar at $T = 1073 \text{ K}$. We found $D_{\text{Ga}}(1 \text{ bar}) = (5.778 \pm 0.124) \cdot 10^{-9} \text{ m}^2 \text{ s}^{-1}$ vs. $D_{\text{Ga}}(0 \text{ bar}) = (5.905 \pm 0.142) \cdot 10^{-9} \text{ m}^2 \text{ s}^{-1}$ for gallium and $D_{\text{Ni}}(1 \text{ bar}) = (3.474 \pm 0.567) \cdot 10^{-9} \text{ m}^2 \text{ s}^{-1}$ vs. $D_{\text{Ni}}(0 \text{ bar}) = (3.762 \pm 0.824) \cdot 10^{-9} \text{ m}^2 \text{ s}^{-1}$ for nickel. The diffusion coefficient decreased by about 2% for Ga and about 8% for Ni with increasing pressure, which is an expected result as the fluid density increases with increasing pressure. The change is, however, small and within the error bars.

Furthermore, the incoherent ISFs were calculated for this alloy at $T = 1073 \text{ K}$ from MD trajectories using the nMOL-DYN3 software [18, 20]. For several Q -values the ISFs are visualized in figure 6 by lines of different color and width. Thin dashed lines correspond to ten separate MD simulation runs and the corresponding thick solid lines represent their average values. Numerical ISFs of separate simulation runs strongly scatter at large times because of the correspondingly low statistics. However, the average values agree well with

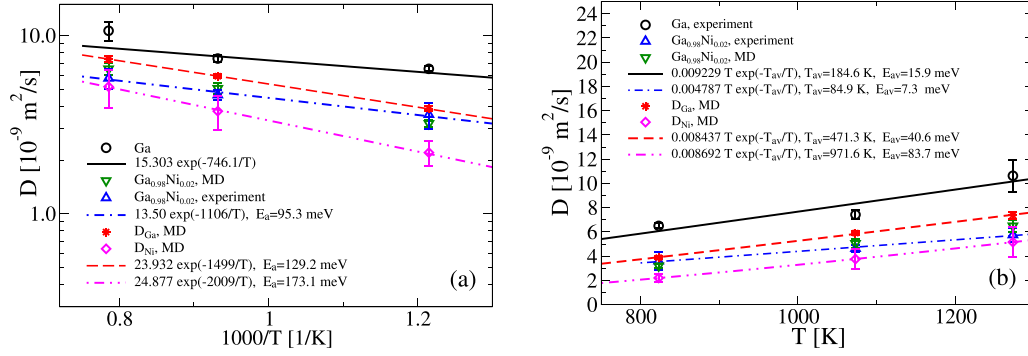


Figure 5. (a) Arrhenius plot for diffusion coefficients (cf legend) of the liquid Ga_{0.98} Ni_{0.02} alloy and of pure liquid gallium. Experimentally derived values of an integral diffusion coefficient of all atoms in the alloy (blue up-pointing triangles) agree well within error bars with the results stemming from MD simulations done with ML-FFs (dark green down-pointing triangles). The latter were obtained from MD diffusion coefficients for gallium (red asterisks), D_{Ga} , and nickel (magenta diamonds), D_{Ni} , upon taking a weighted sum $D = 0.6D_{\text{Ga}} + 0.4D_{\text{Ni}}$ reflecting relative contributions of these two different chemical species to QENS spectra in the investigated alloy (cf text). The blue dash-dotted line presents an Arrhenius fit to the experimental integral diffusion coefficient, whereas the red dashed line and magenta dash-double-dotted line present Arrhenius fits of the theoretical results for Ga and Ni atoms, respectively. The corresponding activation energies and prefactors are given in the legend. (b) Linear plot of the results presented in (a) and their fits with an Einstein-Stokes dependence with the corresponding activation energies and prefactors given in the legend.

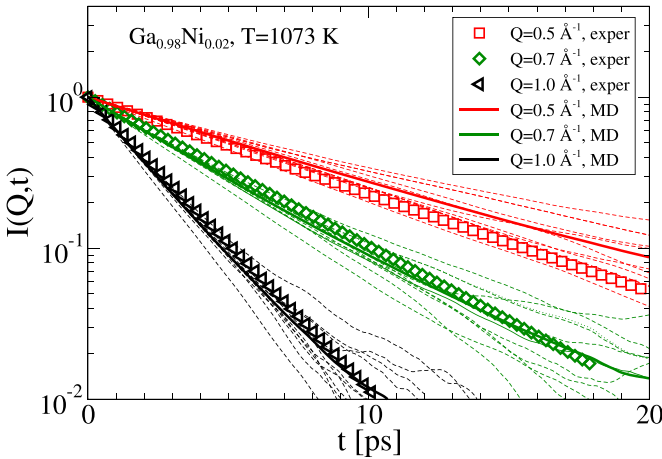


Figure 6. Incoherent intermediate scattering function of Ga_{0.98} Ni_{0.02} liquid alloy plotted as a function of time at $T = 1073 \text{ K}$ for several Q -values (symbols). Thin dashed lines represent the results obtained from ten runs of ML-FF simulations. Thick full lines represent the ensemble averages. The agreement between the averaged MD results and the experimental data is remarkably good for $Q = 0.7 \text{ \AA}^{-1}$ and $Q = 1.0 \text{ \AA}^{-1}$. For $Q = 0.5 \text{ \AA}^{-1}$, the agreement is less good but still in the range of the MD simulation statistical error.

the experimental results exemplary plotted with symbols for $Q = 0.7 \text{ \AA}^{-1}$ and $Q = 1.0 \text{ \AA}^{-1}$ in figure 6. For $Q = 0.5 \text{ \AA}^{-1}$, the average values deviate from the experimental result but are still within the statistical fluctuations.

One of the most striking features is that the diffusion coefficient of gallium in the alloy of 98 at% of gallium with only 2 at% of nickel is significantly smaller than that in pure gallium at the corresponding temperatures. This is not the common case since at such a low concentration of Ni addition, one would expect that the melt properties, including molar volume or packing fraction, stay the same, and, hence, the diffusion coefficient should stay the same. Indeed, the density

of alloy at the same temperature, e.g. 1073 K, with only 2% of Ni, is significantly, about 10%, lower than the density of Ga at the same temperature, see figure 1 of [41] and the corresponding discussion. Moreover, the coordination number of the first coordination shell of Ga reduces in this case from 9.8 to 8.5 [41]. Both intuitively and following the excess entropy scaling theory, this should even increase diffusivity rather than reduce it [41]. Hence, a strong reduction of D_{Ga} is strikingly counter-intuitive. This might have to do with the bonding nature between Ga and Ni and is likely associated with a change of the microscopic structure of the liquid, which needs to be studied further and is beyond the scope of the present work. We only wish to remark that the study of the radial distribution functions $g_{\alpha\beta}(r)$ ($\alpha, \beta = \text{Ga, Ni}$) derived from our MD simulations reveals [41] that the first maximum of $g_{\text{GaNi}}(r)$ occurs at $\sigma_{\text{GaNi}} = 0.2425 \text{ nm}$ much shorter than the position of the first maximum $\sigma_{\text{GaGa}} = 0.2725 \text{ nm}$ of $g_{\text{GaGa}}(r)$, and the maximum value $g_{\text{GaNi}}(\sigma_{\text{GaNi}}) = 3.7871$ is essentially larger than $g_{\text{GaGa}}(\sigma_{\text{GaGa}}) = 2.1448$. It implies that the sparse Ni atoms are more tightly surrounded by Ga atoms than Ga atoms do [41]. In a videoclip of visualized MD dynamics corresponding to 40 ps duration of physical time provided at [41], one can observe temporally highly correlated movements of Ni atoms with the surrounding Ga atoms. Ni atoms also seem to make time from time short-living dimers; see the videoclip. The first maximum of $g_{\text{NiNi}}(r)$ is located at $\sigma_{\text{NiNi}} = 0.2525 \text{ nm}$ in figure 8 of [41] and $g_{\text{NiNi}}(\sigma_{\text{NiNi}}) = 0.9567$ is not essentially smaller than the second and third maxima of this distribution function, which also agrees with our observations. Overall, a multi-peak structure in $g_{\text{NiNi}}(r)$ indicates a local order in the position of Ni atoms. It is astounding, given only 20 Ni atoms in simulations as compared with 980 Ga atoms, which somehow mediate the emergence of this local Ni order. All this points in the direction of locally existing temporal clustering order and requires a further investigation of a highly collective and correlated nature of diffusion processes in GaNi alloys.

Moreover, our results do not exclude that at higher temperatures the diffusion coefficient of gallium in the alloy can even exceed its diffusion coefficient in pure gallium at the same temperature. One can come to this supposition upon extrapolating the corresponding linear fitting dependencies in figure 5(a) to lower $1000T^{-1}$ values. It would happen for $T > 1700$ K, given the fitting parameters in this plot.

5.4. Temperature dependence of the diffusion coefficient of a liquid gallium-nickel alloy

The integral diffusion coefficient measured by QENS exhibits an Arrhenius dependence (equation (9)) with an activation energy $E_a = 95.3$ meV and $D_0 = 13.50 \cdot 10^{-9} \text{ m}^2 \text{ s}^{-1}$ as it is visualized in figure 5(a). Alternatively, it can also be fitted using equation (12) leading to a significantly smaller activation energy $E_{av} = 7.3$ meV, cf figure 5(b). Interestingly, the diffusion coefficients of Ga and Ni achieved from the MD simulations possess much larger and different activation energies in the Arrhenius fit, $E_a = 129.2$ meV and $E_a = 173.1$ meV, respectively, cf figure 5(a). However, the corresponding prefactors D_0 are rather similar: $D_0 \approx 23.9 \cdot 10^{-9} \text{ m}^2 \text{ s}^{-1}$ for Ga and $D_0 \approx 24.9 \cdot 10^{-9} \text{ m}^2 \text{ s}^{-1}$ for Ni. The activation energy for pure nickel is essentially larger in a QENS experiment ($E_a = 470 \pm 30$ meV) with a significantly larger $D_0 = (77 \pm 8) \cdot 10^{-9} \text{ m}^2 \text{ s}^{-1}$ [8]. This implies that extrapolated to temperatures in our experiment and simulations, equation (9) would yield a much smaller D_{Ni} , e.g. $D_{\text{Ni}} = 1.06 \cdot 10^{-9} \text{ m}^2 \text{ s}^{-1}$ at $T = 1273$ K. This is about five times smaller compared to the values found by our MD simulations at the same temperature. Thus, assuming the validity of the Arrhenius behavior for supercooled nickel as observed in [8] down to very low temperatures, nickel seems to diffuse much faster in a GaNi-alloy at low nickel concentration as in pure (heavily supercooled) liquid nickel at the same temperature.

The same effect as described above for gallium rich $\text{Ga}_{1-x}\text{Ni}_x$ liquid alloys is observed in silicon-rich $\text{Si}_{1-x}\text{Ni}_x$ liquid alloys, where the self-diffusion coefficient of nickel is by a factor of about five larger compared to the value for pure nickel indicating that the nickel diffusion is highly coupled to the silicon diffusion [9]. In this case, the activation energy $E_a = 280 \pm 30$ meV was found to be independent of the alloy composition, but, in contrast, the prefactor D_0 depended on the alloy composition and was much larger than the value observed in pure nickel at the same temperatures [9]. This diffusion activation energy was also reduced compared to the activation energy of pure nickel. However, it was essentially larger than the value observed for the $\text{Ga}_{0.98}\text{Ni}_{0.02}$ alloy studied here by MD simulations.

The fit of the MD data by equation (12) visualized in figure 5(b) yields activation energies of $E_{av} = 40.6$ meV for Ga and $E_a = 83.7$ meV for Ni with very similar mobilities $\mu_0 = 6.111 \cdot 10^{11} \text{ s kg}^{-1}$ (Ga) and $\mu_0 = 6.296 \cdot 10^{11} \text{ s kg}^{-1}$ (Ni). Remarkably, in this case (and interpretation) the viscosity activation energy of gallium is indeed very close to the value of the pure gallium on the macroscale [40]. At first glance, it is a striking agreement. However, if this interpretation were fully correct, the diffusion of the diluted nickel atoms would

also reflect the temperature dependence of the viscosity of surrounding gallium liquid. However, it is not the case. In addition to this, the similarity of temperature-independent prefactors for Ga and Ni self-diffusion coefficients despite rather different activation energies—independently of interpretation with either equation (9) or equation (12) - is an interesting observation. It is in line with the excess entropy scaling theory. However, this theory cannot be justified overall for the considered alloy [41]. It needs to be checked and clarified for other Ni concentrations and compositions in future research. A physical theory to explain these complexities represents a genuine challenge for further investigation.

6. Conclusions

The diffusional processes in liquid natural gallium and the gallium rich gallium-nickel alloy $\text{Ga}_{0.98}\text{Ni}_{0.02}$ were studied experimentally using QENS and theoretically based on MD simulations. It was demonstrated that chemical incoherence is negligible for neutron scattering for the systems studied. Despite the small concentration of nickel its contribution to the QENS signal is about 40% and the integral diffusion coefficient of atoms in the alloy as observed by QENS represents a weighted sum of the diffusion coefficients of gallium (about 60%) and nickel (about 40%). The experimental results for pure gallium and MD simulations agree very well in the temperature range between 360 K and 473 K. But also at 340 K and 873 K the observed discrepancies were found to be very small. However, for temperatures above 1000 K the diffusion coefficients determined from the MD simulations were found to increase faster with temperature than the experimentally observed values.

It was demonstrated that MD simulations based on ML-FFs can be used as a reliable substitute for computationally very costly *ab-initio* MD simulations. Due to their linear scaling with system size, ML-FF-MD simulations allow for a significantly larger number of particles and hence larger simulated systems, as well as longer simulation time scales and therefore reduced statistical errors at the same computational costs. This, in turn, allows to find the diffusion coefficient of highly diluted Ni atoms in the liquid matrix of Ga atoms. ML-FF-MD and AIMD simulations essentially agreed within the error bars. However, ML-FF-MD systematically overestimates diffusion coefficients compared to AIMD by less than 6%.

The existing excess entropy scaling theories were shown to overestimate the diffusion coefficient of gallium by a factor of three to four. However, their small modification with a prefactor chosen as the classical Boltzmann diffusion constant fitted the experimental data remarkably well. Moreover, the MD simulation results were excellently described by the Einstein-Stokes formula, with an effective diameter of gallium atoms corresponding to the position of the first maximum of the radial distribution function found in the MD simulations, and a liquid viscosity exponentially dependent on temperature, in agreement with the known experimental data on gallium viscosity, although with a slightly different activation energy. Moreover, the activation energies in the alternative

descriptions are generally different, which is explained by different temperature dependences of the prefactors in the competing theories.

In the case of the GaNi alloy, ML-FF-MD also agreed with the experimental results in the temperature range from 823 K to 1273 K within the error bars. From the presented experimental data, the values of D_{Ga} and D_{Ni} cannot be determined separately. However, these diffusion coefficients could be determined by MD simulations reliably validated by the experimental data for the integral diffusion coefficient. It turns out that the diffusion of gallium is significantly reduced compared to its value in pure liquid gallium at the studied temperatures. However, on an absolute temperature scale the diffusion coefficient of nickel is significantly larger than expected by an extrapolation via the temperature dependence of the diffusion coefficient of pure nickel by equation (9) using the data in [8].

In the case of the studied gallium-nickel alloy, the existing excess entropy scaling theories failed completely to explain our findings on a strong reduction of the gallium diffusion coefficient in the alloy, even with a modification that was successful for gallium liquid alone. We assume that this is due to temporally highly correlated motions of Ni atoms with the surrounding Ga atoms and their dynamical clustering. The study of radial distribution functions obtained from MD simulations revealed that the sparse Ni atoms are more tightly surrounded by Ga atoms than Ga atoms. The emerging puzzle opens a venue for further research.

Data availability statement

The data that support the findings of this study are openly available at the following URL/DOI: <https://zenodo.org/doi:10.5281/zenodo.10302508>.

Acknowledgments

The authors acknowledge support by the Deutsche Forschungsgemeinschaft (DFG) through Project-ID 431791331 - CRC 1452 (Catalysis at Liquid Interfaces, CLINT). This work was also supported by the consortium DAPHNE4NFDI in the context of the work of the NFDI e.V. The consortium is funded by the DFG—Project number 460248799. F Y and W P acknowledge funding through the DFG Grant Nos. PE580/20–4 and YA418/1–4, and thank Sandro Szabo for assistance.

Conflict of interest

The authors declare no conflict of interests.

Appendix

Ga density used in simulations was calculated following [40] as

$$\rho(T) = \rho_0 - \kappa(T - T_{\text{ref}}) \quad (\text{A1})$$

with $\rho_0 = 6077 \text{ kg m}^{-3}$, $\kappa = 0.611 \text{ kg (m}^{-3}\text{K)}$, $T_{\text{ref}} = 302.914 \text{ K}$, cf table A1. The sizes of MD simulation boxes containing 343 Ga atoms were calculated accordingly. They are also given in table A1.

Table A1. Ga densities obtained from equation (A1) at different temperatures, and the corresponding lengths of cubic box including 343 atoms.

T (K)	ρ (kg m ⁻³)	ρ (amu Å ⁻³)	b (Å)
340	6054.340 454	3.646 009	18.719 065
360	6042.120 454	3.638 650	18.731 676
380	6029.900 454	3.631 291	18.744 321
400	6017.780 454	3.623 932	18.757 000
420	6005.460 454	3.616 573	18.769 714
473	5973.077 454	3.597 071	18.803 573
823	5759.227 454	3.468 288	19.033 487
1073	5606.577 454	3.376 300	19.204 798
1273	5484.277 454	3.302 709	19.346 391

ORCID iDs

F Yang  <https://orcid.org/0000-0001-5281-2957>

C Neiss  <https://orcid.org/0000-0001-7213-0187>

I Goychuk  <https://orcid.org/0000-0002-6818-9159>

T Unruh  <https://orcid.org/0000-0002-8903-4850>

References

- [1] Taccardi N *et al* 2017 *Nat. Chem.* **9** 862
- [2] Hofer A *et al* 2023 *RSC Adv.* **13** 4011–8
- [3] Søgaard A, de Oliveira A L, Taccardi N, Haumann M and Wasserscheid P 2021 *Catal. Sci. Technol.* **11** 7535–9
- [4] Levine I R 2009 *Physical Chemistry* 6th edn (McGraw Hill)
- [5] Squires G L 1978 *Introduction to the Theory of Thermal Neutron Scattering* (Dover)
- [6] Boothroyd A T 2020 *Principles of Neutron Scattering From Condensed Matter* (Oxford University Press)
- [7] Price D L and Fernandez-Alonso F F 2013 An introduction to neutron scattering *Neutron Scattering – Fundamentals Experimental Methods in the Physical Sciences* vol 44 F F ed Fernandez-Alonso and D L Price (Academic)
- [8] Meyer A, Stüber S, Holland-Moritz D, Heinen O and Unruh T 2008 *Phys. Rev. B* **77** 092201 (available at: <https://journals.aps.org/prb/abstract/10.1103/PhysRevB.77.092201>)
- [9] Pommrich A I, Meyer A, Holland-Moritz D and Unruh T 2008 *Appl. Phys. Lett.* **92** 241922
- [10] Meyer A 2015 *EPJ Web Conf.* **83** 01002
- [11] Blagoveshchenskii N, Novikov A, Puchkov A, Savostin V and Sobolev O 2015 *EPJ Web Conf.* **83** 02018
- [12] Demmel F, Hennet L, Brassamin S, Neuville D R, Kozaily J and Koza M M 2016 *Phys. Rev. B* **94** 014206
- [13] Meyer A, Hennig L, Kargl F and Unruh T 2019 *J. Phys.: Cond. Matter* **31** 395401
- [14] Weis H, Kargl F, Kolbe M, Koza M M, Unruh T and Meyer A 2019 *J. Phys.: Cond. Matter* **31** 455101
- [15] Embs J P, Juranyi F and Hempelmann R 2010 *Z. Phys. Chem.* **224** 5–32
- [16] Sears V F 1992 *Neutron News* **3** 26–37
- [17] Stüber S 2009 Diffusion dynamics in liquid and undercooled Al-Ni alloys *Ph.D. thesis* Technical University Munich (available at: <https://mediatum.ub.tum.de/739515>)

- [18] Róg T, Murzyn K, Hinsin K and Kneller G R 2003 *J. Comput. Chem.* **24** 657–67
- [19] Calandrini V, Pellegrini E, Calligari P, Hinsin K and Kneller G 2011 *Collect. SFN* **12** 201–32
- [20] Hinsin K, Pellegrini E, Stachura S and Kneller G R 2012 *J. Comput. Chem.* **33** 2043–8
- [21] Frida-1 (available at: <https://jugit.fz-juelich.de/mlz/frida/-/blob/main/wiki/frida1/start.md>)
- [22] Unruh T, Neuhaus J and Petry W 2007 *Nucl. Instr. Meth. Phys. Res. Sec. A* **580** 1414–22
- [23] Mesot J, Janssen S, Holitzner L and Hempelmann R 1996 *J. Neutron. Res.* **3** 293–310
- [24] Shahzad A 2024 Atomic diffusion in liquid gallium and gallium-nickel alloys probed by quasielastic neutron scattering and molecular dynamic simulations, Zenodo (available at: <https://zenodo.org/doi:10.5281/zenodo.10302508>)
- [25] Kresse G and Hafner J 1993 *Phys. Rev. B* **47** 558–61 (available at: <https://journals.aps.org/prb/abstract/10.1103/PhysRevB.47.558>)
- [26] Kresse G and Hafner J 1994 *Phys. Rev. B* **49** 14251–69 (available at: <https://journals.aps.org/prb/abstract/10.1103/PhysRevB.49.14251>)
- [27] Kresse G and Furthmüller J 1996 *Comput. Math. Sci.* **6** 15–50
- [28] Kresse G and Furthmüller J 1996 *Phys. Rev. B* **54** 11169–86
- [29] Jinnouchi R, Lahnsteiner J, Karsai F, Kresse G and Bokdam M 2019 *Phys. Rev. Lett.* **122** 225701
- [30] Jinnouchi R, Karsai F and Kresse G 2019 *Phys. Rev. B* **100** 014105
- [31] Jinnouchi R, Karsai F, Verdi C, Asahi R and Kresse G 2020 *J. Chem. Phys.* **152** 234102
- [32] Kresse G and Joubert D 1999 *Phys. Rev. B* **59** 1758–75
- [33] Perdew J P, Burke K and Ernzerhof M 1996 *Phys. Rev. Lett.* **77** 3865–8
- [34] Methfessel M and Paxton A T 1989 *Phys. Rev. B* **40** 3616–21 (available at: <https://journals.aps.org/prb/abstract/10.1103/PhysRevB.40.3616>)
- [35] Parrinello M and Rahman A 1980 *Phys. Rev. Lett.* **45** 1196–9
- [36] Parrinello M and Rahman A 1981 *J. Appl. Phys.* **52** 7182–90
- [37] Nosé S 1984 *J. Chem. Phys.* **81** 511–9
- [38] Hoover W G 1985 *Phys. Rev. A* **31** 1695–7
- [39] Nosé S 1991 *Progr. Theor. Phys. Suppl.* **103** 1–46
- [40] Assael M J, Armyra I J, Brillo J, Stankus S V, Wu J and Wakeham W A 2012 *J. Phys. Chem. Ref. Data* **41** 033101
- [41] Supplemental material
- [42] Xiong L et al 2017 *Acta Mater.* **128** 304–12
- [43] Mitchell M, Muftakhidinov B and Winchen T Engauge Digitizer Software (available at: <http://markummittchell.github.io/engauge-digitizer>)
- [44] Dyre J C 2018 *J. Chem. Phys.* **149** 210901
- [45] Rosenfeld Y 1977 *Phys. Rev. A* **15** 2545–9
- [46] Dzugutov M 1996 *Nature* **381** 137–9
- [47] Rosenfeld Y 1999 *J. Phys.: Cond. Matter* **11** 5415
- [48] Dzugutov M 2001 *Nature* **411** 720
- [49] Hoyt J J, Asta M and Sadigh B 2000 *Phys. Rev. Lett.* **85** 594–7
- [50] Samanta A, Ali S M and Ghosh S K 2001 *Phys. Rev. Lett.* **87** 245901
- [51] Chapman S and Cowling T G 1939 *The Mathematical Theory of Non-Uniform Gases* (Cambridge University Press)
- [52] Bastea S 2004 *Phys. Rev. Lett.* **93** 199603
- [53] Petit J and Nachtrieb N H 1956 *J. Chem. Phys.* **24** 1027–8